Effects of the Nature and Combinations of Solvents in the Intercalation of Clay with Block Copolymers on the Properties of Polymer Nanocomposites

Sinan Şen,[1] Nihan Nugay,[2] Turgut Nugay[2]

[1]*Advanced Technologies Research and Development Center, Boğaziçi University, 34342 Bebek, Istanbul, Turkey*
[2]*Department of Chemistry and Polymer Research Center, Boğaziçi University, 34342 Bebek, Istanbul, Turkey*

Received 14 January 2008; accepted 8 October 2008
DOI 10.1002/app.29389
Published online 18 December 2008 in Wiley InterScience (www.interscience.wiley.com).

ABSTRACT: Polystyrene (PS) nanocomposites were prepared by the free-radical polymerization of styrene in the presence of organically modified montmorillonite (MMT) clays. MMT clay was modified with a low-molecular-weight and quarternized block copolymer of styrene and 4-vinylpyridine [poly(styrene-*b*-4-vinylpyridine) (SVP)] with 36.4 wt % PS and 63.6 wt % poly(4-vinylpyridine) (P4VP). Special attention was paid to the modification, which was carried out in different compositions of a solvent mixture of tetrahydrofuran (THF) and water. The swelling behavior of the MMT clay was studied by an X-ray diffraction technique. The diffraction peak shifted to lower 2θ angles for all of the modified clays, which indicated the intercalation of the quarternized SVP copolymer into the MMT layers in different degrees. Higher interlayer distances, which showed a high degree of block copolymer insertion, were obtained for solvent compositions with THF in water. The resultant nanocomposites were characterized by X-ray diffraction, atomic force microscopy, scanning electron microscopy, thermogravimetric analysis, and dynamic mechanical analysis. The desired exfoliated nanocomposite structure was achieved when the MMT modification was conducted in 50 or 66 wt % THF, whereas the other modifications all resulted in intercalated structures. The resulting exfoliated nanocomposite was found to have better thermal stability and dynamic mechanical performance compared to the others, even with 2% clay loading.
 J Appl Polym Sci 112: 52–63, 2009

Key words: atomic force microscopy (AFM); block copolymers; mechanical properties; nanocomposites; polystyrene

INTRODUCTION

Polymer/layered silicate or clay nanocomposites possess attractive properties compared to neat polymers and microcomposites.[1] Layered silicate nanofillers have drawn a lot of attention because of their small size or large surface with nanoscale dimensions, which result in enhanced mechanical properties,[2–5] barrier properties,[6,7] thermal stability, and flame-retardant capabilities.[8–11] Hydrophobic behavior and an increase in the spacing between sheets of layer–lattice silicates are two of the most important factors for silicates used as nanocomposite fillers. Ion exchange in the intermediate layers is the usual method for obtaining hydrophobic behavior and an increase in spacing for layered silicates. To make clays compatible with polymers, inorganic cations are replaced by organic onium ions via ion exchange. This also increases the spacing between the silicate layers, which, in turn, promotes the penetration of polymer chains or precursors into the space between the silicate layers.[12–17] Polymer nanocomposites with layered clay ion-exchanged with various organic cations have been widely studied.[1] As alternatives to organic cations, the use of polymeric intercalants, both in the form of homopolymers such as amine-terminated polystyrene (PS)[18] and block copolymers such as poly(ethylene oxide-*b*-styrene), poly(ethylene oxide-*b*-methyl methacrylate),[19] and quaternary salt of 4-vinylpyridine based block copolymers,[20–22] has been given in literature. Although the performances of nanocomposites produced with block copolymer intercalants have been discussed in terms of their block length and nature in these studies, it is thought that there may be some critical insertion parameters also related to the size and nature of block copolymer associates, depending on selective solvent and solvent combinations.

This article reports the effect of solvent mixture and solvent compositions in clay intercalation with block copolymers in polymer nanocomposite formation. In this study, PS–montmorillonite (MMT) clay nanocomposites were synthesized via an *in situ* free-radical polymerization method. MMT clay was

Correspondence to: S. Şen (sensinan@boun.edu.tr).
Contract grant sponsor: Turkish Scientific and Technical Research Center; contract grant number: (TUBITAK project) 107T445.

modified with a low-molecular-weight diblock copolymer of matrix-compatible styrene and quarternized 4-vinylpyridine [poly(styrene-*b*-4-vinylpyridine) (SVP)] in different water/tetrahydrofuran (THF) solvent mixtures. Through the use of a block copolymer intercalant whose non-ionic segment would act as a spacer when the ionized block interacted with the clay surface, we expected to increase the distance between silicate layers, depending on the selective solvent and solvent mixtures in which the block copolymer exhibited different behavior. The nanocomposites with different structures, as intercalated and exfoliated, are discussed in detail in terms of morphology and dynamic mechanical and thermal properties.

EXPERIMENTAL

Materials

4-Vinylpyridine and styrene (Aldrich) were dried over CaH_2 (Aldrich, Steinheim, Germany), distilled *in vacuo*, and stored under nitrogen at −20°C. Styrene was then treated with fluorenyllithium for 15 min and distilled *in vacuo* just before the polymerization. 4-Vinylpyridine was treated with a mirror of sodium under nitrogen and distilled *in vacuo* just before the polymerization. MMT [Nanofil 1080; cationic (Na^+) exchange capacity = 100 mequiv/100 g] was kindly donated by Süd-Chemie (Moosburg, Germany). 2,2′-Azoisobutyronitrile (AIBN) was obtained from Merck (Darmstadt, Germany) and dried *in vacuo* at room temperature. THF (Merck) was purified by refluxing over a sodium–benzophenone complex under dry nitrogen, with a deep purple color indicating a solvent free of oxygen and moisture. The initiator used to prepare the diblock copolymers was *n*-butyllithium (Aldrich, Steinheim, Germany) and was used as received.

Synthesis of the quarternized SVP diblock copolymer

The SVP diblock copolymer was prepared by anionic polymerization with *n*-butyllithium as an initiator in a preflamed glass reactor. The polymerization was designed to give a number-average molecular weight around 6000. The monomers, solvent, and initiator were transferred by syringe and capillary techniques. The reaction was carried out in THF at −78°C. The polymer was terminated with methanol, recovered by precipitation in ether, and dried under vacuum oven at 50°C for 48 h. The resulting block copolymer, SVP, was found to have 36.40 wt % PS and 63.60 wt % P4VP. Its number-average molecular weight was calculated as 7083. A 3 wt % solution of the block copolymer in THF was quarternized with methyl iodide at 50°C for 24 h under a nitrogen atmosphere.[23] The quarternized product, polystyrene-*block*-poly(*N*-methyl-4-vinylpyridinium iodide) copolymer, was then precipitated in ether and dried *in vacuo* at 50°C. The detailed characterization of the SVP block copolymer and its quarternized form was reported previously.[21]

TABLE I
Modified MMTs and Their PS Nanocomposites

Water/THF in MMT modification	Organophilic MMT	PS nanocomposite
100/0	SVP(W)MMT	PS–SVP(W)
80/20	SVP(20THF)MMT	PS–SVP(20THF)
50/50	SVP(50THF)MMT	PS–SVP(50THF)
33/66	SVP(66THF)MMT	PS–SVP(66THF)
0/100	SVP(THF)MMT	PS–SVP(THF)

Modification of MMT

MMT (2 g) was dispersed in 300 mL of deionized water at 80°C, and a separate solution of 1.16 g of quarternized SVP in 300 mL of deionized water was heated and mixed at 80°C for 1 h. Then, the polymer solution was slowly added to the clay solution and mixed vigorously while the temperature of the solution was kept at 80°C. After mixing, the total volume was brought up to 800 mL, and the solution was stirred for 5 h. We recovered the organically modified MMT by filtering the solution followed by repeated washings of the filter cake with deionized water to remove excess ions. The final product was dried at 50°C in a vacuum oven for 48 h. Organophilic MMTs were also obtained with quarternized SVP copolymer through an ion-exchange reaction by the same procedure but in a solvent mixture of THF and water in different compositions with the volume of the total solvent retained. The solvent composition is given in Table I.

Preparation of the PS nanocomposites

Organophilic MMTs (2 wt % of monomer) were mixed with styrene monomer at 40°C for 5 h. The AIBN initiator (1 wt % of monomer) was added to the mixture and dissolved. Then, the polymerization reaction was carried out at 65°C for 48 h to obtain polymer nanocomposites whose nomenclature is given in Table I.

Methods

X-ray diffraction (XRD) analysis

To measure the basal spacing (d_{001} reflection) of the MMT clays, wide-angle XRD measurements were conducted on a Rigaku D/Max-Ultimate diffractometer (Rigaku, Tokyo, Japan) with Cu Kα radiation

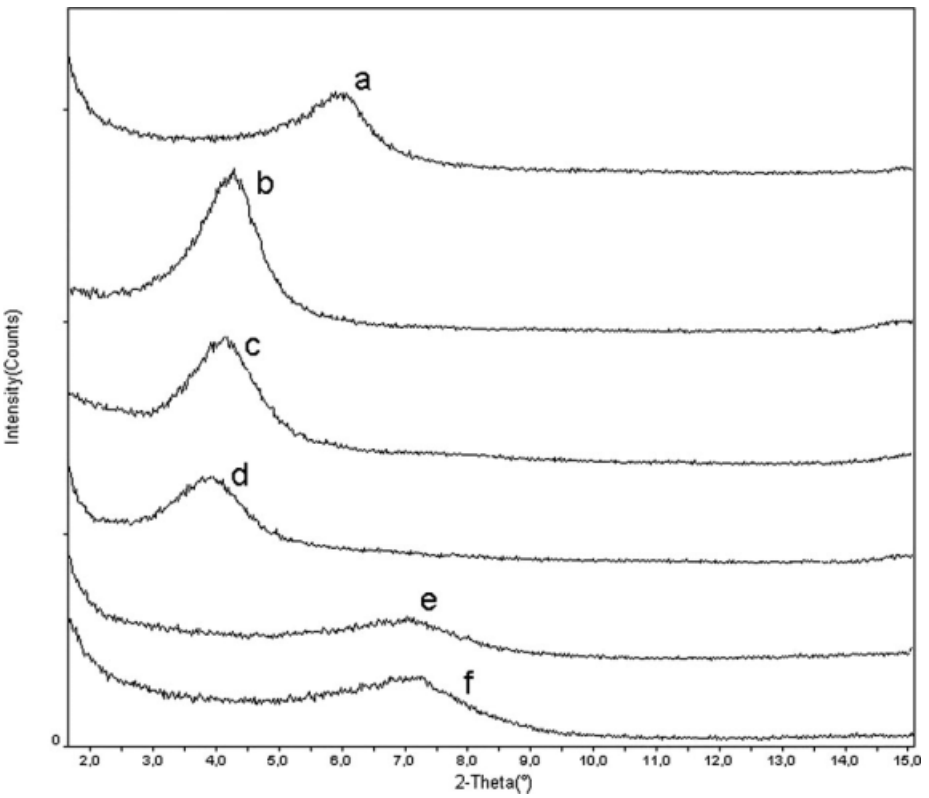

Figure 1 XRD curves of (a) SVP(W)MMT, (b) SVP(20THF)MMT, (c) SVP(50THF)MMT, (d) SVP(66THF)MMT, (e) SVP(THF)MMT, and (f) NaMMT.

(wavelength = 1.54 Å) operating at 40 kV and 40 mA.

Particle size distribution

Multimodal size distribution (MSD) analysis of the block copolymer solution was done on a 90Plus particle size analyzer (Brookhaven Instruments, New York). The technique we used, photon correlation spectroscopy of quasi-elastically scattered light, is based on the correlation of the fluctuations about the average, scattered, laser light intensity. For the measurement, the copolymer was diluted in THF and water mixture at different ratios, in which MMT clay was modified, with concentrations varying from 3 to 0.01 mg/mL. The samples run at the highest concentrations were diluted and remeasured until an optimized autocorrelation function, which was independent of concentration, was obtained.

TABLE II
XRD Data for the Clays and P4VP Nanocomposites

	d_{001} (Å)[a]	
Clay	Clay	Nanocomposite
NaMMT	12.13 (7.28°)	
SVP(W)MMT	14.76 (5.98°)	14.17 (6.22°)
SVP(20THF)MMT	20.72 (4.26°)	15.46 (5.71°)
SVP(50THF)MMT	21.43 (4.12°)	No reflection
SVP(66THF)MMT	22.86 (3.86°)	No reflection
SVP(THF)MMT	12.69 (6.95°)	15.47 (5.70°)

[a] 2θ angles are given in parentheses.

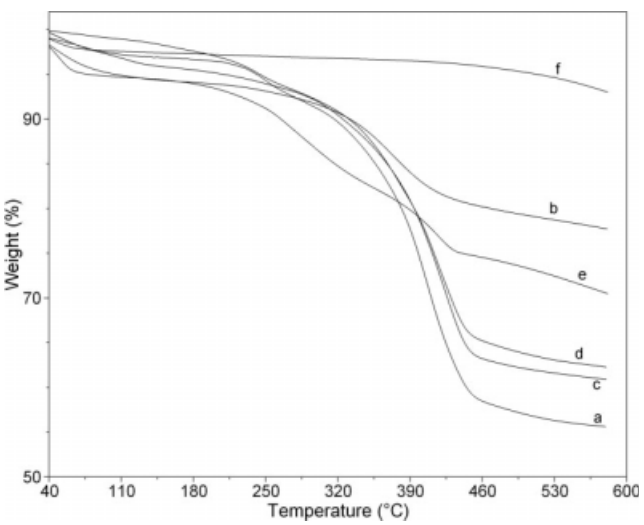

Figure 2 TGA thermograms of (a) SVP(W)MMT, (b) SVP(20THF)MMT, (c) SVP(50THF)MMT, (d) SVP(66THF)MMT, (e) SVP(THF)MMT, and (f) NaMMT.

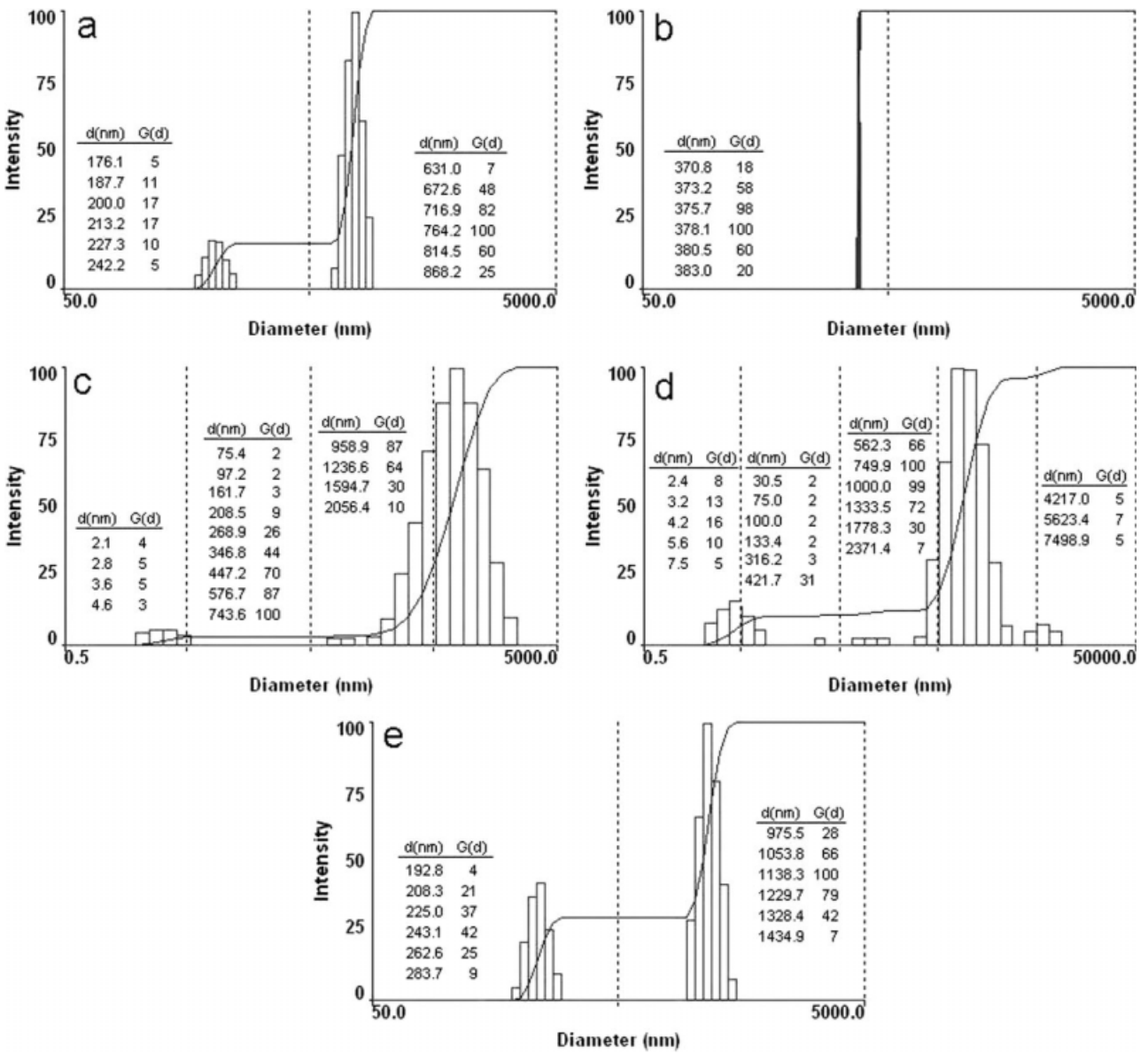

Figure 3 MSD of the SVP block copolymer colloidal particles in THF/water solvent mixtures: (a) 0/100, (b) 20/80, (c) 50/50, (d) 66/33, and (e) 100/0.

Thermogravimetric analysis (TGA)

TGA was performed on TA Instruments TGA-Q50 instrument (TA Instruments, New Castle, DE) under a nitrogen flow at a heating rate of 10°C/min.

Dynamic mechanical analysis (DMA)

The dynamic mechanical properties of the composites were measured with a dynamic mechanical analyzer (DMA Q800, TA Instruments) in single-cantilever mode at a frequency of 1 Hz and at a heating rate of 3°C/min. The samples for the DMA experiments were compression-molded into rectangular shapes at elevated temperatures and a pressure of about 1.72 MPa. The average dimensions of the molded samples were $12 \times 35 \times 3$ mm^3.

Scanning electron microscopy (SEM)

The fracture surfaces of the composites were investigated by SEM analysis with a Philips XL-30 ESEM-FEG/EDAX microscope (Philips, Eindhoven, The Netherlands).

Atomic force microscopy (AFM)

AFM was performed with a universal scanning probe microscope (Ambios Technology, Santa Cruz, CA). Phase-mode imaging was performed with a silicon nitride cantilever probe with a nominal resonance

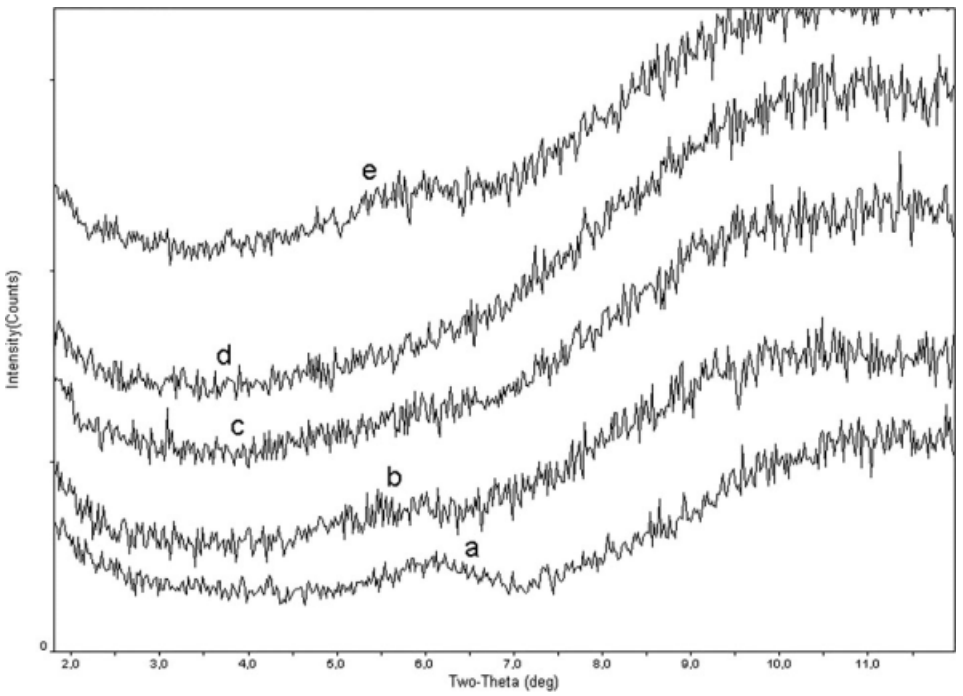

Figure 4 XRD curves of (a) PS–SVP(W), (b) PS–SVP(20THF), (c) PS–SVP(50THF), (d) PS–SVP(66THF), and (e) PS–SVP(THF).

frequency around 170 kHz and a nominal tip radius of 5–10 nm. We prepared samples for AFM investigation by first sectioning the molded sample, mounting it in epoxy potting compound, and then etching it with an acid mixture of HNO_3 and HCl.

RESULTS AND DISCUSSION

The MMT modification was investigated via XRD analysis (Fig. 1). The diffraction patterns were collected between 1 and 15° with a scanning rate of 2°/min. The basal spacing of MMT was obtained from the peak position of the d_{001} reflection in the XRD pattern. The XRD data of the modified clays showed 001 basal spacing enlargement, as indicated in Table II, which indicated that the intercalation of the SVP into the MMT in all of the solvent compositions was successful. The higher interlayer distance observed in SVP(66THF)MMT (Table II) was attributed to the possible better spacer action of the PS segment in high THF medium because THF is a good solvent for PS. On the other hand, in pure water and THF solvents, the possible formation of micelles with comparatively larger PS and quarternized P4VP cores, respectively, inhibited the insertion of the block copolymers into interlayer galleries most probably via potentially good ion-exchange ability but poor swelling in the former, as opposed to good swelling but weak ion-exchange ability in the latter.

The modification of the MMT clay was also confirmed by TGA, and the data are given in Figure 2. It is clear from the figure that all of the modified MMT clays showed lower decomposition onset temperatures and higher degradation-dependent weight losses compared to NaMMT. This result was accepted as an indication of the successful modification of the MMT clay. Moreover, as expected, depending on the solvent nature and combination, different block copolymer amounts between the galleries were observed. Most probably, this was due to the different sized aggregates of block copolymer formation in solution, which led to different diffusion power in the interlayer galleries.

Figure 3 shows the MSD analysis of the SVP block copolymer colloidal particles in different solvent compositions. In MSD analysis, information about the particle sizes and the corresponding values of intensity weighted sizes, positions of the peaks, and ratios of the peak areas are obtained. As shown by the size distribution graphs, the SVP copolymer exhibited particle sizes of 2.1–4.6 nm with a relative intensity of 17 in the solvent mixture having 50% THF [Fig. 3(c)], whereas in the solvent mixture having 66% THF [Fig. 3(d)], these particle sizes reached 2.4–7.5 nm with a relative intensity of 52. On the other hand, in other copolymer solutions, the previously mentioned small particle sizes were not achieved; only very big aggregates, up to 2–7 μm, were obtained.

The highest expansion values for the SVP(50THF)MMT and SVP(66THF)MMT clay layers were attributed to the formation of much smaller aggregations in the corresponding solvent mixtures,

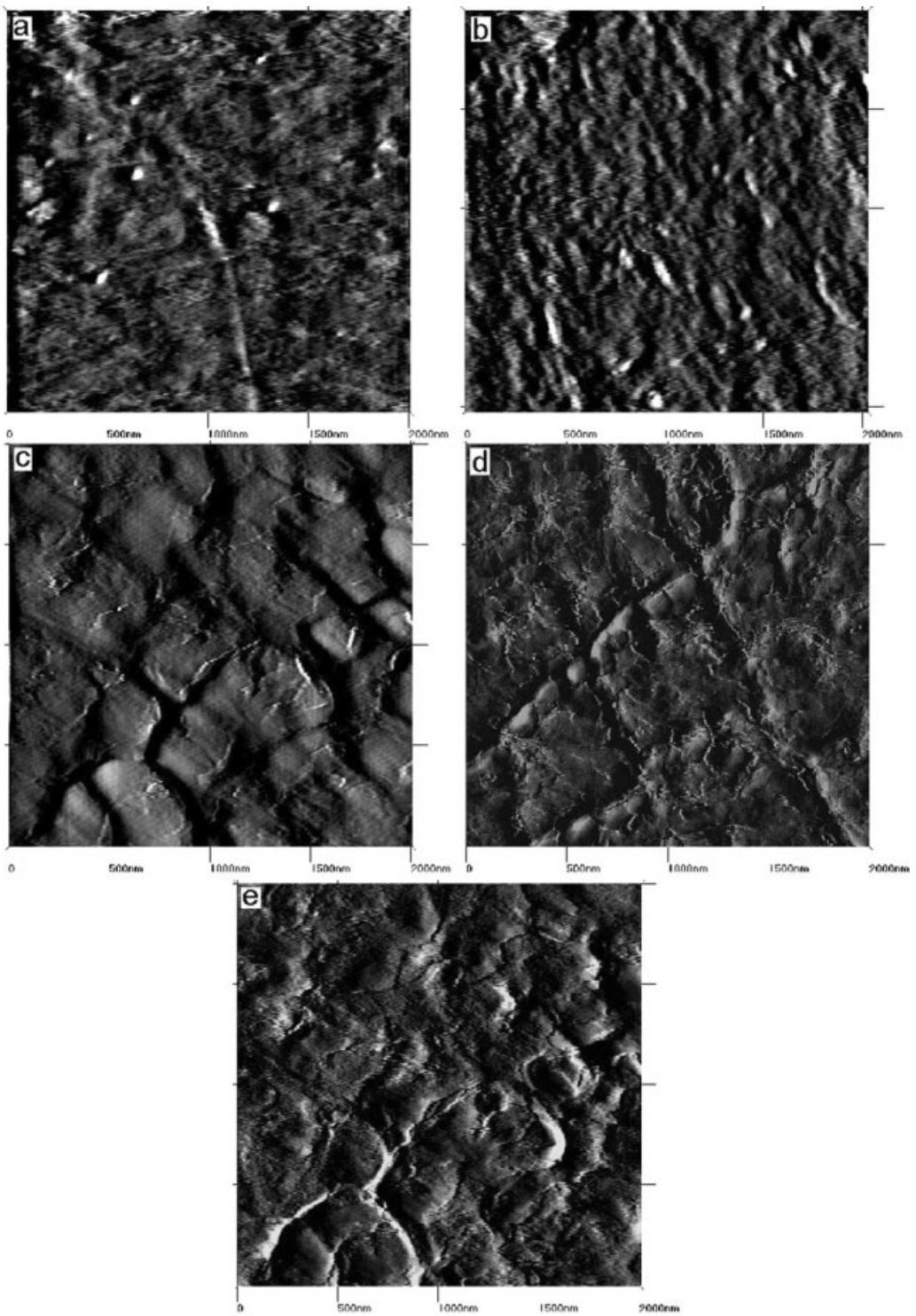

Figure 5 AFM phase images (scan size = 2 μm) of (a) PS–SVP(W), (b) PS–SVP(20THF), (c) PS–SVP(50THF), (d) PS–SVP(66THF), and (e) PS–SVP(THF) nanocomposites.

which led to successful insertion between the interlayer galleries. It was quite obvious that these block copolymers, which exhibited a small number of tiny copolymer chains, gave rise to the expansion of clay layers most probably because of their more diffusive character. This initial expansion, then, led to the insertion of other medium-sized copolymers (ca. 300–400 nm) in later stages of clay modification. These results were found to be very well correlated with the TGA data of these modified clays with comparatively high amounts of SVP copolymer. Of course, there may have also been another method of

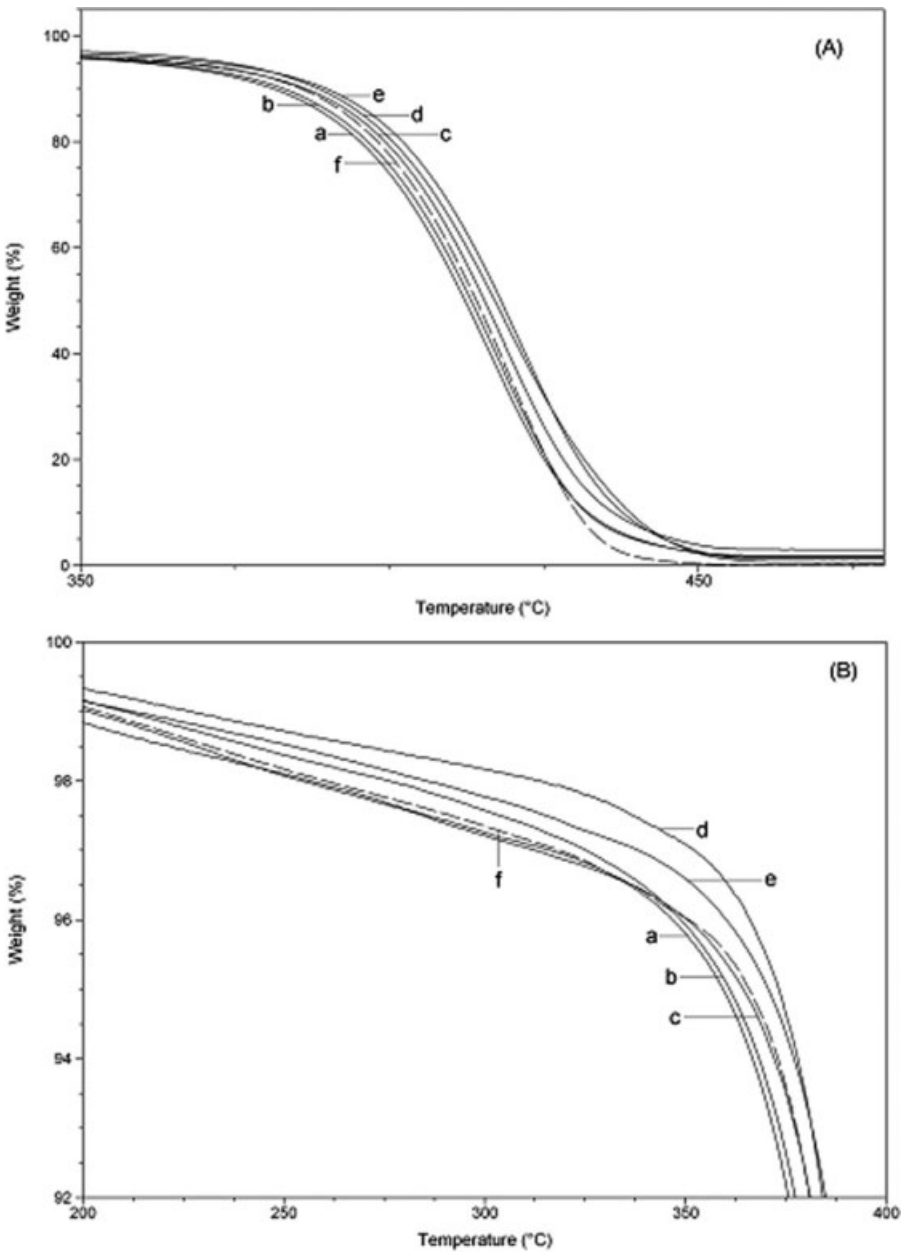

Figure 6 TGA thermograms of (a) PS–SVP(W), (b) PS–SVP(20THF), (c) PS–SVP(50THF), (d) PS–SVP(66THF), (e) PS–SVP(THF), and (f) PS.

contribution to organophilization for the block copolymers via edge–surface interactions rather than interlayer interaction with clay. However, the much larger sized aggregates, on the other hand, seemed to be ineffective in organophilization and washed away during the washing step of the modification. These results were in good agreement with the aforementioned TGA data (Fig. 2). Although the SVP(20THF)MMT clay had a higher expansion value (Table II), some of the block copolymers from interlayer galleries could be removed most probably by the large amount of water in the solvent mixture

TABLE III
TGA Data for the Neat PS and PS Nanocomposites

Material	T_{d5} (°C)	T_{d50} (°C)	Maximum rate of weight loss (%/°C)
PS	365.84	414.02	2.65
PS–SVP(W)	359.36	412.18	2.44
PS–SVP(20THF)	361.04	413.18	2.51
PS–SVP(50THF)	366.44	415.33	2.50
PS–SVP(66THF)	373.26	417.02	2.27
PS–SVP(THF)	370.65	418.00	2.49

T_{d5} = temperature at which 5% degradation occurs; T_{d50} = midpoint degradation temperature.

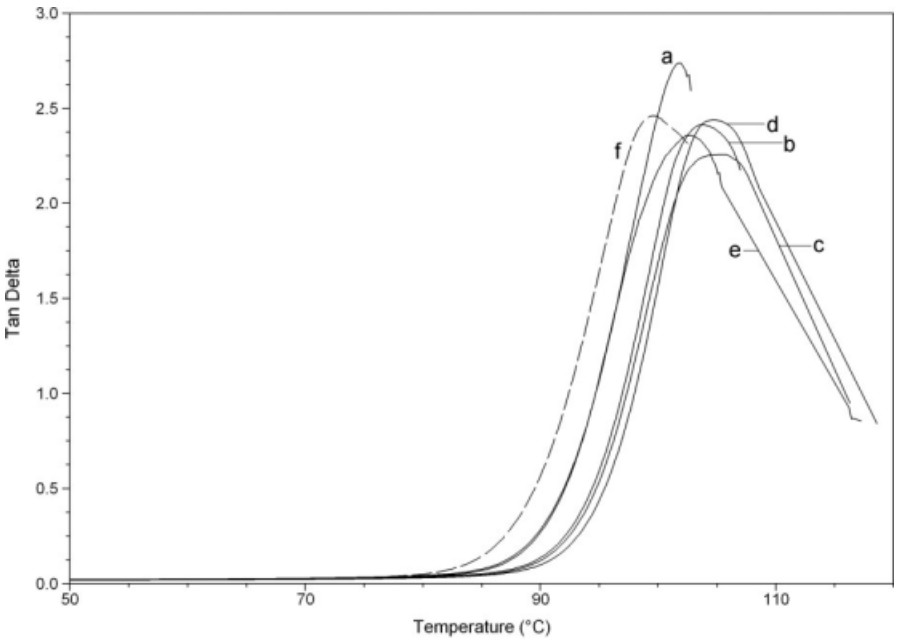

Figure 7 Tan δ versus temperature plots for (a) PS–SVP(W), (b) PS–SVP(20THF), (c) PS–SVP(50THF), (d) PS–SVP(66THF), (e) PS–SVP(THF), and (f) PS.

during the washing step, which was also confirmed by the low amount of SVP in the TGA data.

The dispersion of modified clays in PS was investigated with the XRD technique. (Fig. 4 and Table II). Among the others, only the nanocomposites PS–SVP(50THF) and PS–SVP(66THF) did not show a noticeable peak appearing in the XRD region. This result strongly indicates that the corresponding silicate layers were exfoliated and homogeneously dispersed in the PS matrix. The exfoliated nanocomposite structure most probably resulted from the interaction of a high amount of styrene monomer with the block copolymer with a much more opened form of PS segment, which consequently led to the complete dispersion of the clay layers in the matrix. On the other hand, all of the other PS nanocomposites exhibited a peak in the relevant angle region representing the diffraction from the (001) crystal surface of the silicate layers of the organoclay as an indication of intercalated nanocomposite

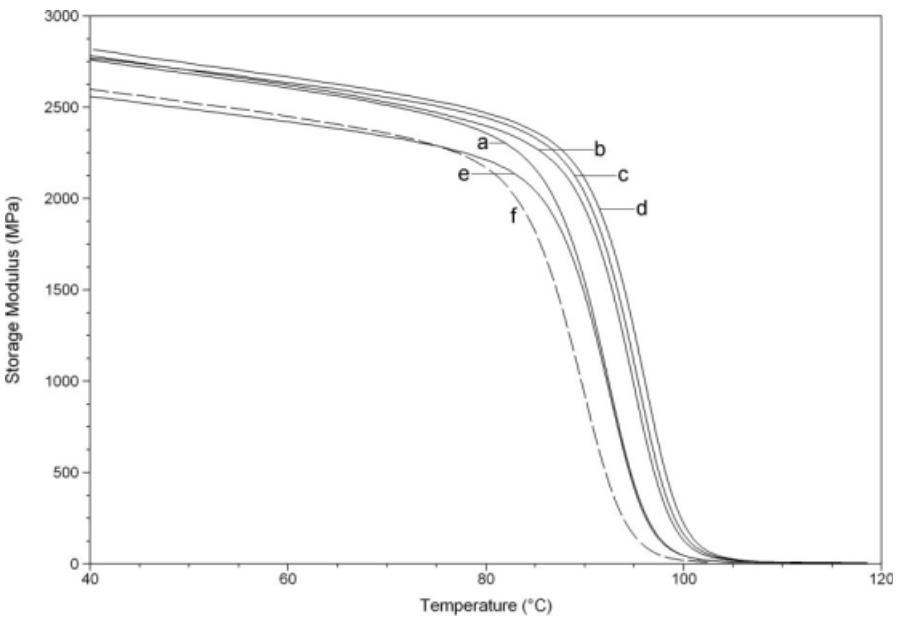

Figure 8 Storage modulus versus temperature plots for (a) PS–SVP(W), (b) PS–SVP(20THF), (c) PS–SVP(50THF), (d) PS–SVP(66THF), (e) PS–SVP(THF), and (f) PS.

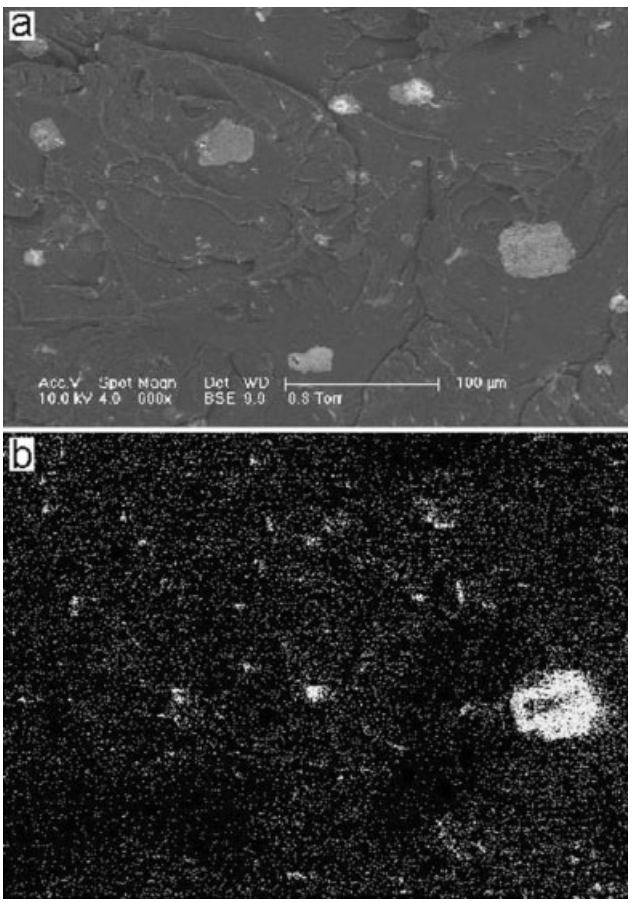

Figure 9 (a) SEM image of the fracture surface of PS–SVP(W) and (b) X-ray scan for silicon in the same area.

structures. Although the SVP(20THF)MMT clay had one of the highest swelling degrees, its nanocomposite showed an organoclay peak. In this solvent composition (20/80 THF/water), although the interlayer galleries were quite expanded in modification, during nanocomposite formation, a small amount of block copolymer (Fig. 2) with a compact styrene segment between the galleries accepted the styrene monomer in lower amounts, and the residual water between the layers may have repelled the added styrene monomer. This may have led to the exclusion of block copolymer chains from the interlayer galleries, which resulted in a decrease in the distance between layers. Moreover, the relatively smaller and broader nature of this peak could be accepted as proof of the existence of a partially exfoliated or intercalated structure.[12] In terms of the SVP(THF)MMT clay, both the existence of a certain amount of clay intercalation via the peak shift from 12.13 to 12.69 Å and TGA confirmation (Fig. 2) showed the successful organophilization of MMT layers from interlayer galleries and the edges/surfaces of the clay. During nanocomposite formation, the possible pulling of silica layers with the styrene monomer through the edge–surface-attached styrene-compatible block copolymers may have contributed to further intercalation (15.47 Å).

To determine the morphology of the nanocomposites, the AFM results were examined. AFM analysis of polymer nanocomposites has been widely used to investigate clay dispersion in polymer matrices. Especially in the tapping mode AFM, the phase contrast in the image is caused by repulsive probe-tip–sample interactions with the nanosilica, which result in a positive phase and bright areas or features corresponding to the nanosilica–clay phase.[24,25] Figure 5(a–d) shows the AFM images of the surface-etched nanocomposites in the phase mode. AFM verified nanoscale and homogeneous dispersions of the SVP(66THF)MMT and SVP(50THF)MMT clays in the matrix [Fig. 5(c,d)]. Moreover, exfoliation was quite clear, and silica nanoplatelets with a thickness of about 20 nm were oriented in all possible directions to one another in the matrix as further confirmation of the XRD peak disappearance. On the other hand, large clay aggregates (ca. 90–100 nm in size), together with a few small aggregates, in the matrices were observed for other composites [Fig. 5(a,b,e)], which may have been due to the intercalated structures.

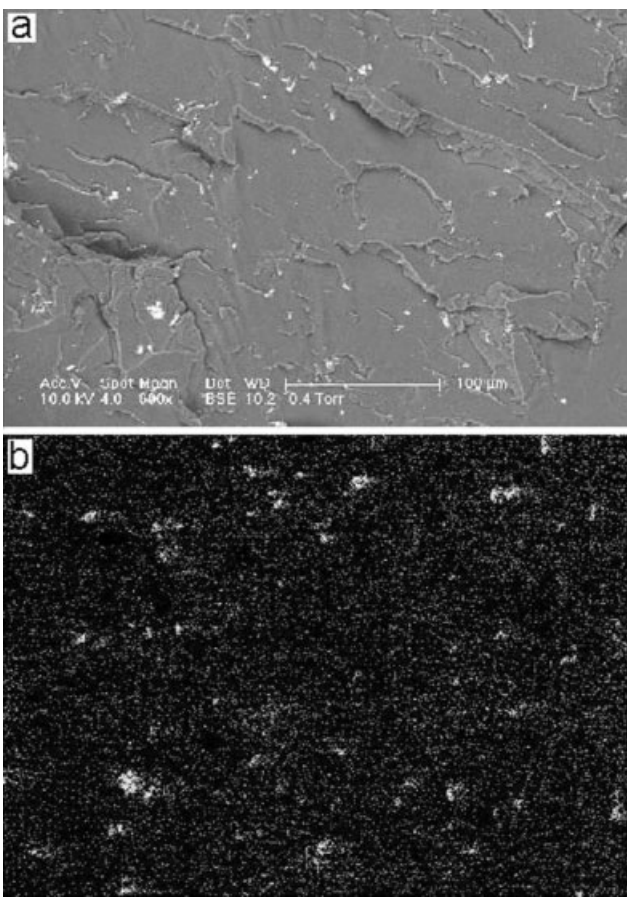

Figure 10 (a) SEM image of the fracture surface of PS–SVP(20THF) and (b) X-ray scan for silicon in the same area.

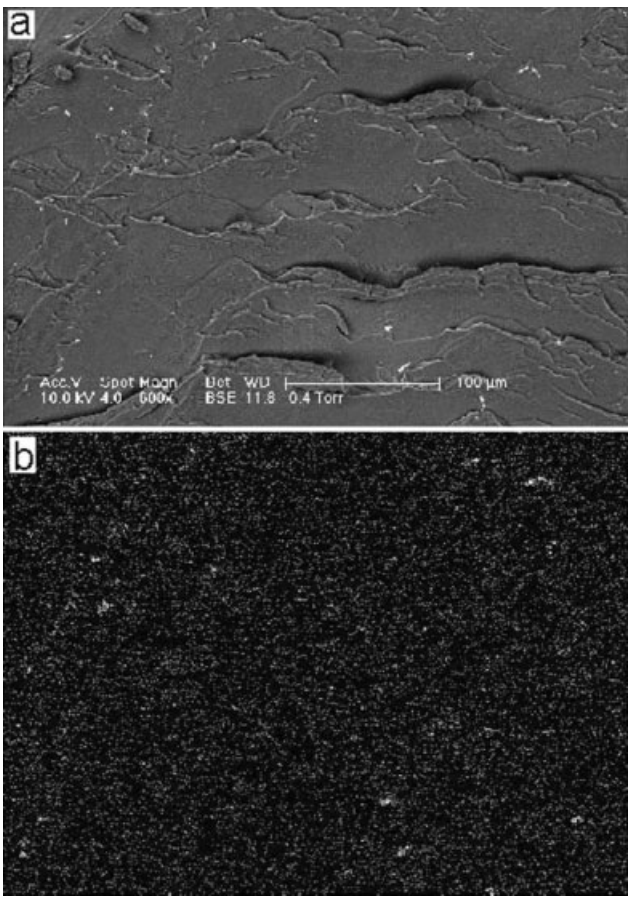

Figure 11 (a) SEM image of the fracture surface of PS–SVP(50THF) and (b) X-ray scan for silicon in the same area.

The TGA data of the samples [Fig. 6(A) and Table III] showed that the polymer nanocomposites, except PS–SVP(W) and PS–SVP(20THF), began to decompose at higher temperatures compared to pure PS. The temperature at which 5% degradation occurred, representative of the onset temperature of degradation, was found to be the highest for PS–SVP(66THF) (Table III). The nanocomposites PS–SVP(66THF) and PS–SVP(50THF), on the other hand, exhibited higher midpoint degradation temperatures, which may have been due to extensive interaction of PS with nanodispersed and large surface area organophilic clays, which then resulted in inhibition of the diffusion of the decomposed product in the polymer matrix. Although the nanocomposite PS–SVP(THF) seemed to have the highest midpoint degradation temperature, it lost its initial weight at a much earlier temperature [Fig. 6(B)]. In addition to the previously mentioned data, as maximum rates of weight loss values for the samples were concerned (Table II), PS–SVP(66THF), with the lowest rate of decomposition, seemed to have the highest thermal stability relative to the other polymer nanocomposites and the "virgin" PS.

The nanocomposites were subjected to DMA to observe their thermomechanical responses. The tan δ versus temperature and storage modulus versus temperature plots are shown in Figures 7 and 8, respectively. The glass-transition temperatures (T_g) of each nanocomposite was taken as the maximum tan δ peak point, which was calculated from the loss modulus/storage modulus ratio.[21,26] Compared to neat PS, all of the nanocomposites were found to have higher tan δ peak temperatures or T_g values, which was also in good agreement with the increase in the storage modulus values shown in Figure 8. The nanocomposite PS–SVP(66THF) was found to have the highest increase in T_g of PS. This may have been due to its exfoliation morphology (Fig. 4), which led to a large surface area of the clay interacting with the polymer and preventing the segmental motions of the polymer chains near organic–inorganic interfaces;[27,28] this was also in agreement with its highest thermal stability (Fig. 6).

The fracture surfaces of the PS nanocomposites were investigated by SEM with backscattered imaging (Figs. 9–13). Figure 9(a,b) illustrates the fracture surface of the PS–SVP(W) composite and the X-ray

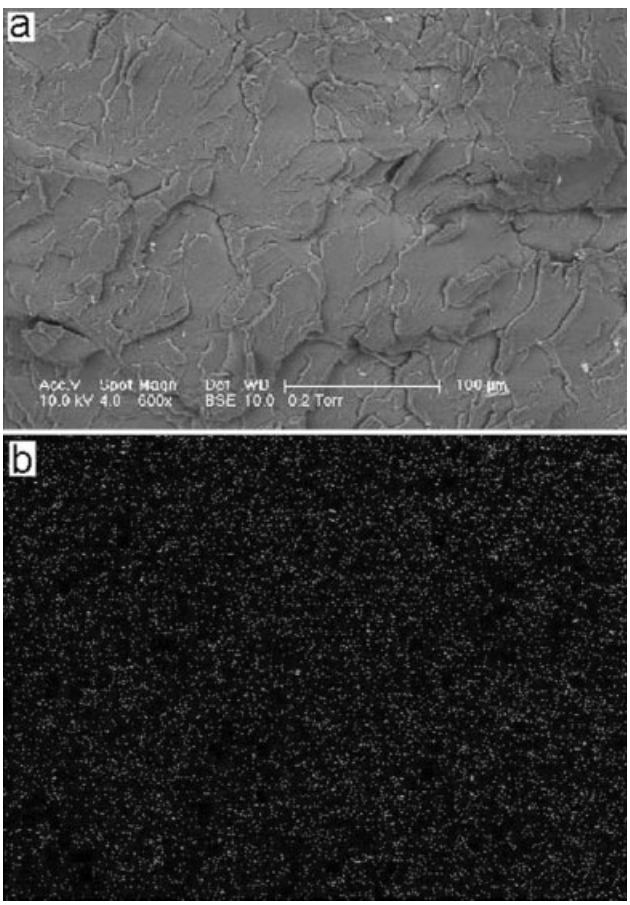

Figure 12 (a) SEM image of the fracture surface of PS–SVP(66THF) and (b) X-ray scan for silicon in the same area.

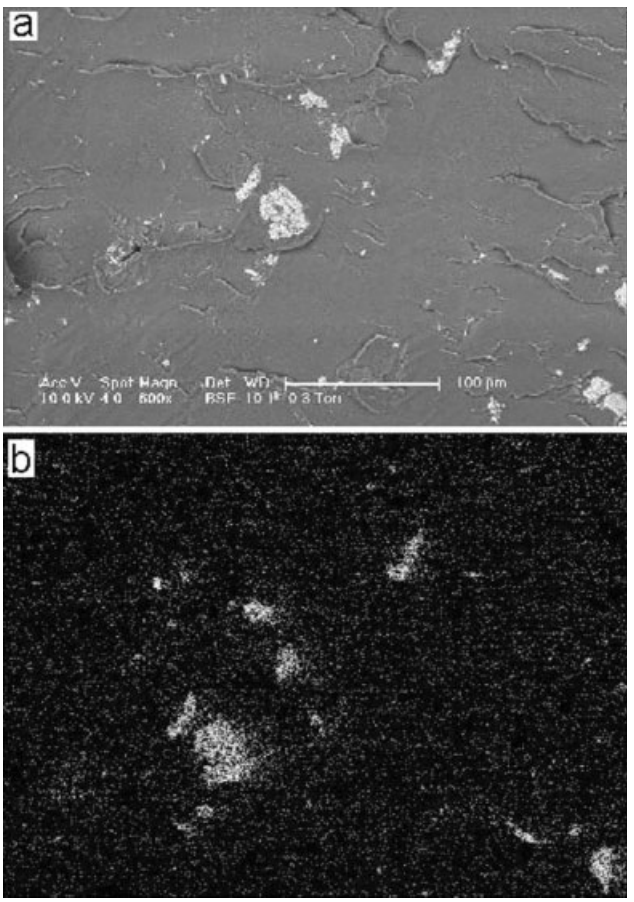

Figure 13 (a) SEM image of the fracture surface of PS–SVP(THF) and (b) X-ray scan for silicon in the same area.

scan for elemental Si of the same area, respectively. These matching images show that the agglomerate corresponded to MMT clay. From Figure 9, one can see large aggregated particles about 16.6 μm size. Also, for the composite PS–SVP(THF), large clay particles about 7.7 μm in size, together with small aggregates, were easily observed (Fig. 13). From these observations, it can be said that, when the clay modification was done in pure water or pure THF, the resulting clays seemed to be poorly dispersed in the matrix. In Figure 10, well-dispersed smaller clay particles around 4.3 μm in size are clearly shown for the PS–SVP(20THF) composite, but they still existed as agglomerates. PS–SVP(50THF) (Fig. 11) had a fracture surface with only a very few smaller agglomerates (ca. 2.8 μm), which may have been due to a partially exfoliated structure of the composite, which was also confirmed by XRD analysis (Fig. 4). On the other hand, the PS–SVP(66THF) composite showed a completely different morphology (Fig. 12). At the same magnification, the fracture surface was not found to have any MMT domains, and the corresponding elemental mapping for silicon did not show any agglomeration, which suggested that the SVP(66THF)MMT agglomerates were dissociated to much smaller particles whose sizes were well below the SEM resolution.[29] This conclusion was in accord with the XRD data that the highest MMT expansion occurred when the clay modification was done in the solvent mixture with 66% THF (Table II), which resulted in exfoliation with the nanoscale dispersion of clays.

In terms of the fracture mechanisms of the composites, the SEM image of PS–SVP(66THF) (Fig. 12) showed a more homogeneous fracture surface with crack propagation along a rougher path, which may have been due to the fine dispersion of the clay layers in the polymer matrix. The other composites were found to have a quite heterogeneous crack formation with different sized cracks and some areas without any crack propagation, most probably due to their intercalated nature.[21,30]

CONCLUSIONS

Solvent-dependent organophilic modification of clay with a quarternized diblock copolymer (SVP) was achieved successfully and confirmed by XRD analysis. It seemed that when THF volume was equal or above 50% in total aqueous solution, the block copolymer served a good spacer because of extended PS segments and good exchange capacity because of the extended and well-positioned quaternized P4VP. The desired exfoliated nanocomposite structures were obtained when the MMT modification was conducted in the presence of 50 and 66% THF in the solution. PS–SVP(66THF), as the most effective exfoliated nanocomposite, showed the highest thermal stability and the best dynamic mechanical responses. This was due to completely delaminated silica layers in the nanoscale, as shown by both the absence of any diffraction peak in the XRD region and the observation of fine particles in the AFM and SEM analyses.

References

1. Ray, S. S.; Okamoto, M. Prog Polym Sci 2003, 28, 1539.
2. Kojima, Y.; Usuki, A.; Kawasumi, M.; Okada, A.; Fukushima, Y.; Kurauchi, T.; Kamigaito, O. J Polym Sci Part A: Polym Chem 1993, 31, 1755.
3. Ke, Y.; Long, C.; Qi, Z. J Appl Polym Sci 1999, 71, 1139.
4. Wang, Z.; Pinnavaia, T. J. Chem Mater 1998, 10, 1820.
5. Zilg, C.; Thomann, R.; Mulhaüpt, R.; Finter, J. Adv Mater 1999, 11, 49.
6. Messersmith, P. B.; Giannelis, E. P. J Polym Sci Part A: Polym Chem 1995, 33, 1047.
7. Yano, K.; Usuki, A.; Okada, A.; Kurauchi, T.; Kamigaito, O. J Polym Sci Part A: Polym Chem 1993, 31, 2943.
8. Doh, J. G.; Cho, J. Polym Bull 1998, 41, 511.
9. Gilman, J. W.; Kashiwagi, T.; Brown, J. E. T.; Lomakin, S. SAMPE J 1997, 33, 40.
10. Gilman, J. W. Appl Clay Sci 1999, 15, 31.

11. Su, S.; Wilkie, C. A. J Polym Sci Part A: Polym Chem 2003, 41, 1124.
12. Alexandre, M.; Dubois, P. Mater Sci Eng 2000, 28, 1.
13. Kojima, Y.; Usuki, A.; Kawasumi, M.; Okada, A.; Fukushima, Y.; Kurauchi, T.; Kamigaito, O. J Mater Res 1993, 8, 1185.
14. Fukushima, Y.; Okada, A.; Kawasumi, M.; Kurauchi, T.; Kamigaito, O. Clay Miner 1988, 23, 27.
15. Usuki, A.; Kojima, Y.; Kawasumi, M.; Okada, A.; Fukushima, Y.; Kurauchi, T.; Kamigaito, O. J Mater Res 1993, 8, 1179.
16. Usuki, A.; Kawasumi, M.; Kojima, Y.; Okada, A.; Kurauchi, T.; Kamigaito, O. J Mater Res 1993, 8, 1174.
17. Lebaron, P. C.; Wang, Z.; Pinnavaia, T. J. Appl Clay Sci 1999, 15, 11.
18. Hoffmann, B.; Dietrich, C.; Thomann, R.; Friedrich, C.; Mülhaupt, R. Macromol Rapid Commun 2000, 21, 57.
19. Fischer, H. R.; Gielgens, L. H.; Koster, T. P. M. Acta Polym 1999, 50, 122.
20. Şen, S.; Nugay, N.; Nugay, T. e-Polymers 2003, No. 49.
21. Şen, S.; Nugay, N.; Nugay, T. Polym Int 2006, 55, 552.
22. Zhang, B. Q.; Chen, G. D.; Pan, C. Y.; Luan, B.; Hong, C. Y. J Appl Polym Sci 2006, 102, 1950.
23. Nguyen, D.; Varshney, S. K.; Williams, C. E.; Eisenberg, S. Macromolecules 1994, 27, 5086.
24. Kashiwagi, T.; Morgan, A. B.; Antonucci, J. M.; VanLandingham, M. R.; Harris, R. H.; Awad, W. H.; Shields, J. R. J Appl Polym Sci 2003, 89, 2072.
25. Reichert, P.; Nitz, H.; Klinke, S.; Brandsch, R.; Thomann, R.; Mülhaupt, R. Macromol Mater Eng 2000, 275, 8.
26. Kim, H. G.; Oh, D. H.; Lee, H. B.; Min, K. E. J Appl Polym Sci 2004, 92, 238.
27. Noh, M. W.; Lee, D. C. Polym Bull 1999, 42, 619.
28. Landry, C. J. T.; Coltrain, B. K.; Landry, M. R. Macromolecules 1993, 26, 3702.
29. Al-Khanbashi, A.; El-Gamal, M.; Moet, A. J Appl Polym Sci 2005, 98, 767.
30. Şen, S.; Memeşa, M.; Nugay, N.; Nugay, T. Polym Int 2006, 55, 216.